KTiOPO$_4$, KTiOAsO$_4$, and KNbO$_3$ crystals for mid-infrared femtosecond optical parametric amplifiers: analysis and comparison

S. Cussat-Blanc[1]**, A. Ivanov**[1]**, D. Lupinski**[2]**, E. Freysz**[1]

[1] CPMOH – Université Bordeaux I, 351 cours de la Libération, 33405 Talence Cedex, France
(Fax: +33-05/5684-6970, E-mail: scussat@cribx1.u-bordeaux.fr)
[2] Cristal Laser, 12 allée Jean-Rostand, BP.44, 54230 Chaligny, France

Abstract. We have designed a simple mid-IR femtosecond OPA seeded by a white-light continuum and delivering very stable, largely tunable and energetic output pulses. This OPA requires fewer than 200 μJ of 120-fs Ti:sapphire pump pulses as energy. This system allowed us to experimentally compare the performances of potassium crystals (KTP, KTA, and KNbO$_3$) for the generation of up to 100-fs Fourier-transform-limited pulses tunable in 1–4.6 μm mid-IR wavelengths.

PACS: 42.65.Yj; 45.65.Re; 42.70.Mp

The development of fs sources working in the spectral domain around 3 μm is important since it makes it possible to study time-resolved infrared vibrational spectroscopy of C-H, N-H, O-H,... fundamental stretching modes which are involved in many physical and chemical as well as biological processes. In recent years, the development of powerful and reliable fs lasers has made optical parametric sources a reality: optical parametric amplifiers (OPA) routinely generating sub-100-fs pulses largely tunable in the near infrared with sup-1-μJ energy pulses now available. Data on the performance of infrared OPA sources have been published [1–3] but to our knowledge, only one attempt in comparing the performances of KTP family crystals has been made [4]. In that study the authors used a fs OPA seeded by a Q-switched Nd-YLF laser and pumped by the tunable output of a Ti:sapphire regenerative amplifier. Such a device has two drawbacks: first the frequency tuning of such an OPA is not convenient since besides the oscillator, it involves re-adjusting many elements in the Ti:sapphire regenerative amplifier. Second, such tuning affects the comparison between the different crystals since it may alter many pump pulse parameters. In the present paper, we propose a theoretical and experimental study of three crystals containing potassium: KTiOPO$_4$ (KTP), KTiOAsO$_4$ (KTA), and KNbO$_3$ using a double-pass fs OPA pumped by the fixed output of a Ti:sapphire regenerative amplifier. This OPA is seeded by a white-light continuum and the frequency tuning is achieved through a rotation of the crystal. The paper is organized in the following way. First, we discuss important crystal parameters such as the phase-matching curves,

group velocities mismatch, and second-order nonlinear effective susceptibility which partly control the amplitude and the temporal and spectral structure of parametrically generated IR fs pulses. Second, we present our very simple experimental OPA setup and the techniques we used to characterize the generated IR pulses. Finally, we discuss our results.

For spectroscopic purposes, the important parameters of IR pulses generated by the OPAs are their high peak power, great stability, and their Fourier-transform-limited (FTL) nature. All are influenced by the characteristics of the crystal used in the OPA. Many fs OPO or OPA systems working in the mid-IR domain (2–5 μm) have been built around one of the three crystals KTP, KTA, and KNbO$_3$, which contain potassium. All these biaxial crystals belong to the $mm2$ point group of symmetry. For fs nonlinear applications, the KTP crystal is well known and has often been used for generating FTL mid-IR pulses in both OPA and OPO [1–3, 5, 6]. It has a very high damage threshold, a good transparency range (0.35–4.5 μm) and high nonlinear coefficient ($d_{32} \approx 2.65$ pm/V). Compared to KTP, the KTA crystal has a higher transparency range (0.35–5.3 μm) and a larger $d_{32} \approx 4.5$ pm/V nonlinear coefficient. Therefore it should make it possible to extend the IR spectral range covered by KTP crystal and improve the overall conversion efficiency. The KNbO$_3$ crystal is known for its large nonlinear effective susceptibility ($d_{32} \approx -13.7$ pm/V) and for its large transparency range (0.4 − 4 μm). Therefore, it could be used to generate more powerful IR fs pulse energy than KTP and KTA crystals but in a smaller IR spectral range if the conclusions drawn in the well-known crystal handbook hold [7]. However, in a real OPA system, we shall see that a simple and direct comparison of the performances of the crystals in our OPA lead us to slightly different conclusions.

1 Theoretical background

To build our OPA system, we first theoretically studied the signal, idler, and pump pulse configuration polarization for mid-IR generation. To compute the cut angles, the optimum thickness, and to determine the spectral tuning range of each

crystal, we used the Sellmeier equations given in [8–10] for KTP, KTA, and $KNbO_3$, respectively. For all crystals, the phase-matching conditions between signal, idler, and pump pulses were computed by considering that all the wave vectors were collinear and that they lie in the (X, Z) plane (i.e. for $\varphi = 0$). In Fig. 1, we show the theoretical evolution of signal and idler wavelengths versus the internal angle (θ) for a fixed pump wavelength ($\lambda_p = 810$ nm). For KTP and KTA, two configurations of polarization are phase matched in the $X - Z$ plane: type-II configuration for which signal (s), idler (i), and pump (p) pulses are, respectively, ordinary (o), extraordinary (e), and ordinary (o) polarized (sip > oeo); and type-III which implies the following polarization configuration: sip $\rightarrow$ eoo. This phenomenon has previously been reported [11]. Note that the type-II configuration which induces the generation of idler wavelengths limited at $\approx 2.7 \, \mu m$ is not suited for fundamental stretching vibrational spectroscopy. The latter requires at least that the OH spectral domain should be covered in a range from 3 to 3.5 μm. Therefore the type-II configuration was not our main interest even if we were experimentally able to observe it. On the other hand, the spectral tuning range presented in Fig. 1a shows that, through a rotation of $\approx 12°$ of the crystal around Y axis, the type-III configurations made it possible to cover the 2–5 μm spectral range. For $KNbO_3$, in the $X - Z$ plane, phase matching occurred only for type-I configuration (i.e. sip $\rightarrow$ ooe). The theoretical angle tuning curve is plotted in straight lines in Fig. 1b. It is interesting to note that tuning the crystal over the whole 2–5 μm spectral range only required a rotation of $\approx 2°$ of the $KNbO_3$ crystal. This is to be compared with the 12° tilt angle for the KTP and KTA crystals. Therefore, the $KNbO_3$ crystal has a wide spectral acceptance. Note the vertical slope of the angle tuning curve near 48.7° indicating a wavelength non-critical phase matching. As a result, very

wide bandwidths are available in this wavelength region. According to these angle tuning curves, we decided to cut the crystals we used so that at normal incidence the central frequency of the idler wave would be centered around 4 μm. The angles of cut (θ, φ) as well as the important parameters of the crystals are reported in Table 1.

The thickness of the crystal is another important OPA parameter to be determined. The optimum thickness is controlled by the group velocity mismatch (GVM) between signal, idler and pump pulses. The GVM is a function of the wavelength. The computed GVM for the three crystals is presented in Fig. 2. We will focus our attention on the 1–1.2 μm spectral range which according to the pump wavelength $\lambda_p = 0.81 \, \mu m$ makes it possible to generate idler waves in the 4.26–2.5 μm fundamental IR stretching frequency of OH and CH groups. We first consider the pump–signal GVM (plotted in open circles in Fig. 2). For KTA, it is about -75 fs/mm in the 1–1.2 μm spectral range whereas for KTP the absolute value of the GVM is smaller than 20 fs/mm over the whole tuning range. For $KNbO_3$, the amplitude of this parameter is larger and steadily increases from 50 fs/mm at 1 μm up to 140 fs/mm at 1.2 μm. Secondly, we consider the signal–idler GVM (plotted in full up triangles in Fig. 2). As signal wavelength increases (i.e. idler wavelength decreases), signal–idler GVM which is about -60 fs/mm and -110 fs/mm at 1 μm for KTP and KTA, respectively, attains a positive value and reaches 90 fs/mm and 70 fs/mm at 1.2 μm for KTP and KTA, respectively. For $KNbO_3$, this parameter is always smaller than 80 fs/mm in the 1–1.6 μm signal tuning range. Finally, let us consider the pump–idler GVM (plotted in straight lines in Fig. 2). For $KNbO_3$ this parameter is around 60 fs/mm at 1 μm, but it rapidly increases and reaches around 230 fs/mm at 1.2 μm. For KTP this GVM is negative and about -50 fs/mm at 1 μm. It is continuously
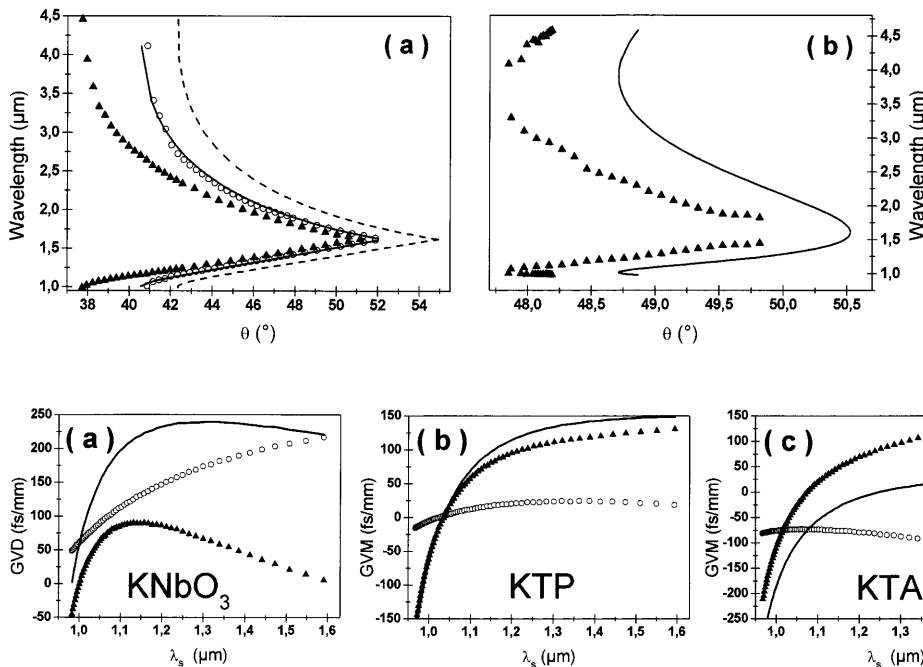
Fig. 1a,b. Theoretical and experimental angle tuning curves for KTP, KTA, and $KNbO_3$. **a** Theoretical and experimental curves were respectively plotted in *straight lines* and *open circles* for KTP and in *dashed lines* and *full upward triangles* for KTA. **b** Theoretical and experimental curves were respectively plotted in *straight lines* and *full upward triangles* for $KNbO_3$

Fig. 2a–c. Theoretical group velocities (v_g^{-1}) mismatches are reported for $KNbO_3$ (**a**), for KTP (**b**), and for KTA (**c**). *Open circles*, *straight lines*, and *full upward triangles* respectively represent $v_{gpump}^{-1} - v_{gsignal}^{-1}$, $v_{gpump}^{-1} - v_{gidler}^{-1}$, and $v_{gsignal}^{-1} - v_{gidler}^{-1}$ in fs/mm

Table 1. Characteristics of KTP, KTA, and KNbO$_3$ crystals are shown. MGVM is the maximum of group velocities mismatches between the three waves calculated for a generated idler wavelength centered at 3.3 μm, l_{eff} is the corresponding pump, signal, and idler pulses interaction length and d_{eff} is the mean value of the second-order nonlinear effective susceptibility

Crystal	Transparency range /μm	Type of interaction	Cut angle $(\theta; \varphi)°$	MGVM / fs/mm at $\lambda_i = 3.3$ μm	l_{eff}/mm at $\lambda_i = 3.3$ μm	d_{eff}/pm/V
KTP	[0.35; 4.5]	III	(40.1; 0)	50	2.4	1.8
KTA	[0.35; 5.3]	II	(42.6; 0)	75	1.6	3.1
KNbO$_3$	[0.4; 5.6]	I	(49; 0)	177	0.7	11.0

shifted positively as the wavelength increases and reaches 120 fs/mm at 1.2 μm. The same behavior is observed for KTA.

Since the pump–signal interaction length is an important parameter for efficient generation of the signal wave, it is clear that a 2-mm crystal length is suitable for both KTP and KTA crystals pumped by 120-fs pulses. For KNbO$_3$ a crystal length of about 1 mm would suffice (see Table 1). However, since we wanted to compare the performances of the three crystals, we also chose a length of 2 mm for KNbO$_3$. For KTP note that all the GVMs are equal to zero around $\lambda_i = 1.05$ μm. This clearly indicates that a longer crystal length can be used for an efficient fs parametric generation around this wavelength. Indeed, at this wavelength, GVM does not limit signal, idler, or pump length interaction. In fact, it is mainly the angular walk-off between the pump signal and idler pulses that is the limiting factor. Moreover, another problem related to the spatial structure of the generated pulses may arise. For such a long crystal and for powerful spatially Gaussian pump pulses, a saturation of the parametric gain as well as total conversion of the pump in the signal and idler or even reconversion of signal and idler wave in the pump wave could occur. Along the propagation axis in the crystal, the point at which the saturation and the re-conversion occur depends on the pump intensity. Hence the nature of the spatial pump beam profile implies that the saturation of the parametric gain and re-conversion signal and idler pulses do not occur at the same point on the beam profile in the crystal. Therefore, at the exit point of the crystal, both saturation of the parametric gain saturation and re-conversion phenomenon should manifest themselves by the occurrence of a transversely ring-shaped pump signal or idler beam in the far field. If this behavior is not desirable, the thickness of KTP crystal must be reduced.

Next, we computed the evolution of the effective second-order nonlinear susceptibility $(\chi_{eff}^{(2)} = 2d_{eff})$ versus signal (or idler) wavelength. The effective nonlinearity was calculated according to $d_{eff} = \sum_{l,m} e_p^l d_{lm}(e_s e_i)^m$ where d_{lm}, e_p^l, and $(e_s e_i^m)$ are the components of the square nonlinearity tensor, the eth component of pump normalized electric field and the mth component of the signal–idler normalized electric field respectively. Note this general expression allows us to compute the d_{eff} whatever the considered type of parametric interaction. In the three crystals and for the chosen type of interaction, d_{eff} decreased as signal wavelength increased from 1 to 1.6 μm. For KNbO$_3$, the d_{eff} (≈ 11 pm/V) change was about ±1%. For the other crystals the change was more pronounced (±10%), and d_{eff} decreased from 1.6 pm/V to 2.0 pm/V and from 2.8 to 3.4 pm/V for KTP and KTA, respectively, in the 1–1.6 μm wavelength range. Therefore, if the interaction length between the signal, pump, and idler pulses is kept constant, the output pulse energy should be more constant over the whole spectral tuning range with KNbO$_3$ compared to KTP or KTA. On the other hand, since the d_{eff} of KNbO$_3$ is about 3.5 and 5.5 larger than that of KTA and KTP, respectively, the use of KNbO$_3$ crystal in our OPA should provide more energetic output pulses compared to KTP and KTA.

2 Experimental set-up

The sketch of our simple OPA setup is presented in Fig. 3 showing all the optical elements of our OPA. The system is based on the double-pass optical parametric amplification of a white-light continuum in a crystal (KTP, KTA, or KNbO$_3$) synchronously pumped by a small part of the energy (185 μJ) of a commercial Ti:sapphire regenerative amplifier working at a 1-kHz repetition rate. The 120-fs pump pulses have their central wavelength at 810 nm. The white-light continuum generated in a 5-mm-thick sapphire optical flat by focusing less than 1 μJ of the Ti:sapphire pulse energy leaking through a mirror. The generated white-light continuum was then collimated to reduce its diameter to about 900 μm on the crystal. The pump arm (see Fig. 3) used most of the Ti:sapphire pulse energy. To reduce the pump beam waist size to ≈ 600 μm in the crystal, the pump pulses passed through an afocal system. The minimum beam-waist size of the pump was limited by the damage threshold of the used crystal. It was about
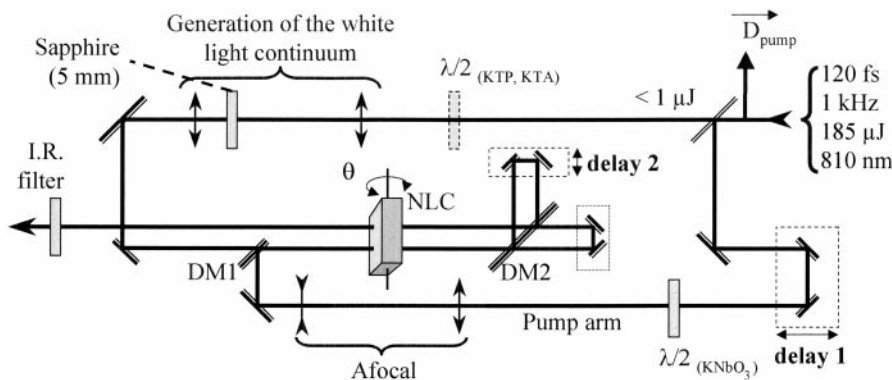
Fig. 3. OPA experimental setup. DM1 and DM2 are dichroic mirrors, NLC is the nonlinear crystal and can be either KTP, KTA, or KNbO$_3$ crystal. A λ/2 plate is placed on the pump arm for KNbO$_3$ crystal or on the continuum arm for KTP and KTA crystals

$400\,\text{GW/cm}^2$ for KTP and KTA and was slightly higher for KNbO$_3$. Pump and continuum beams were spatially superposed by the use of a dichroïc mirror (DM1 in Fig. 3) and were temporally synchronized with a delay line (placed in the pump arm). To achieve a double-pass amplification, the pump beam was separated from the generated signal pulses by a second dichroïc mirror (DM2 in Fig. 3) and sent back synchronously to the crystal by a second delay line. The two-stage amplification produced a good conversion efficiency. Tuning of our OPA is quite simple and requires a rotation of the crystal (around the Y axis, as shown in Fig. 3). After each rotation of the crystal, a slight readjustment of the synchronization between pump and continuum pulses was performed. This was done to compensate the group velocities mismatch between each spectral component occurring during the generation of the white-light continuum in the sapphire crystal and its propagation in the different optical elements of our OPA. Notice the rotation axis of the crystal (Y axis) fixes the polarization directions of the signal, idler, and pump pulses. Therefore, according to the chosen type of interaction in the crystal (see Table 1), a $\lambda/2$ plate must be placed on the pump arm for KNbO$_3$ crystal or on the continuum arm for KTP and KTA crystals.

To characterize the spectrum of IR-generated pulses, a 50-cm imaging spectrometer/monochromator coupled to a CCD matrix sensor or a liquid-nitrogen-cooled InSb sensor was used. The IR pulse duration was measured with a non-collinear lab-made autocorrelator. For mid-IR pulses ($\lambda = 1$–$1.4\,\mu\text{m}$) the second-order autocorrelation was performed by using a 1-mm-thick type-I KDP crystal coupled to a photomultiplier for KTP and KTA OPAs. The poor quantum efficiency of our photomultiplier above $0.7\,\mu\text{m}$, did not allow us to perform the characterization of signal pulses whose wavelengths were higher than $1.4\,\mu\text{m}$ To avoid this problem and in view of the larger pulses energy with KNbO$_3$ OPA than with KTA ones, we used a silicon photodiode instead of the photomultiplier to perform the second-order autocorrelation of MIR pulses generated in KNbO$_3$. The second-order

autocorrelation of idler pulses was more difficult to measure. It was done by using the two-photon absorption induced in a InGaAs photodiode. Note, this autocorrelation can be done only when the photodiode used is transparent at fundamental OPA frequency ω but absorbs at twice the fundamental OPA frequency 2ω. Since InGaAs photodiodes absorb wavelengths up to $\approx 1.7\,\mu\text{m}$, second-order autocorrelation using such photodiodes required the central wavelength of the idler pulses to be higher than $1.8\,\mu\text{m}$. On the other hand, for idler pulses whose central wavelengths are higher than $3.2\,\mu\text{m}$, the two-photon absorption was so weak that it could not be detected. Therefore, idler pulse duration measurements could be performed only within the 1.8–$3.2\,\mu\text{m}$ wavelength range. The signal and idler output pulse energy was measured with a pyroelectric detector known to have a constant spectral responsivity in the near- and mid-infrared spectral range.

3 Experimental results and discussion

For each crystal, the experimental angle tuning curve was obtained. Then we measured the temporal and spectral bandwidths as well as the output pulse energy of signal and idler pulses.

In Fig. 1a, the experimental angle tuning curve is shown for KTP (open circles). The experimental and theoretical angle tuning curves are in very good agreement. For KTP crystal, the recorded signal pulse temporal bandwidth and spectral bandwidth are presented in Fig. 4c as filled triangles and open circles respectively. In Fig. 4c, the dashed lines are only a visual guide. Note a decrease in the pulse duration ($\Delta\tau$) from 80 to 50 fs at full width at half maximum (FWHM) and an increase in spectral bandwidth ($\Delta\tau$) from 27 to 65 fs at FWHM for increasing signal wavelengths. The experimental temporal spectral bandwidth product (TSBP), given by $\text{TSBP} = \Delta\tau_{\text{fs}}\Delta\lambda_{\text{nm}}/1.47 \times 10^{-3}\lambda_{\text{nm}}^2$ and equal to unity for Fourier-transformed-limited (FTL) Gaussian pulses, was equal to 1.0 ± 0.2 over the whole signal spectral range,
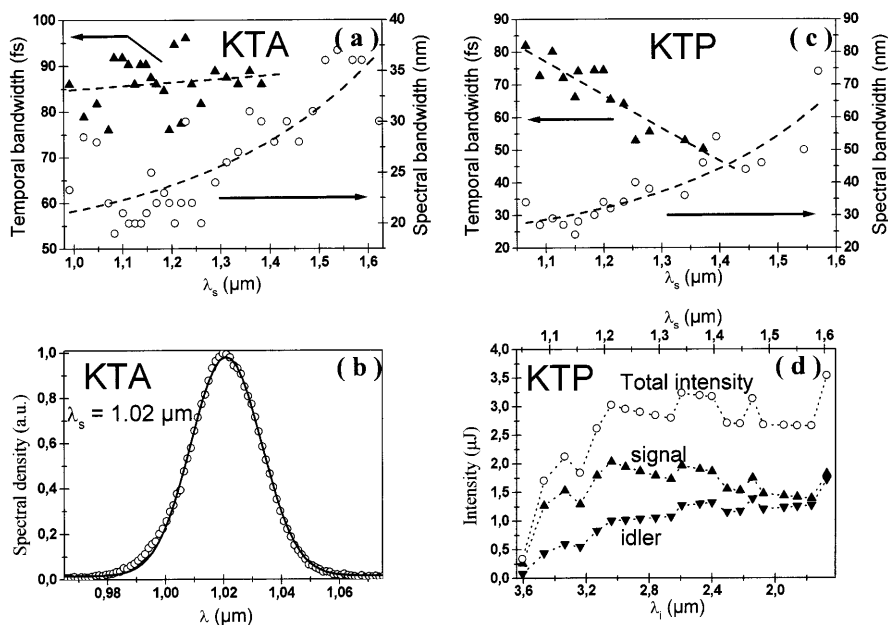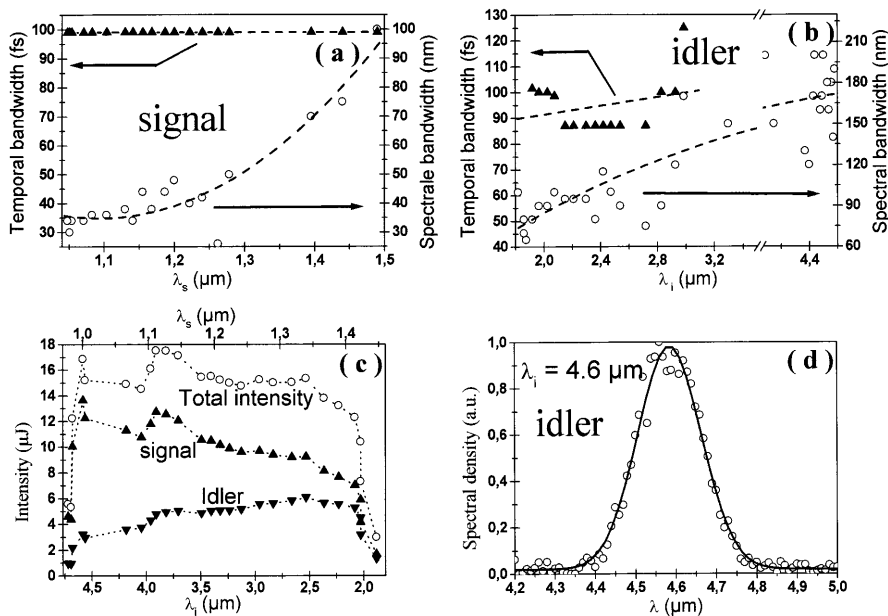

Fig. 4a–d. OPA experimental results obtained with KTA (**a, b**) and KTP (**c, d**) crystals. **a , c** The pulse duration at FWHM (full width at half maxmum) in *full upward triangles* and their spectral bandwidth at FWHM in *open circles*. *Dashed lines* are only a visual guide. **b** A typical signal spectrum (*open circles*) obtained with KTA and centered at $1.02\,\mu\text{m}$ with Gaussian fit (*straight lines*). **d** Total, signal, and idler output pulses energies with KTP are respectively plotted in *open circles*, *full upward* and *downward triangles*

suggesting that the signal pulses were FTL. For idler pulses, we note that as the idler wavelength increased from 1.8 to 3.6 μm, there was a decrease in the pulse duration from 170 to 140 fs at FWHM and an increase in the spectral bandwidth from 30 to 270 nm at FWHM. The idler TSBP was equal to 1.1 ± 0.2. Therefore the idler pulses were slightly less FTL than signal pulses. Finally we measured the output pulse energy of the KTP OPA. In Fig. 4d, the signal output pulse energy versus the wavelength is presented in full upward triangles. It is about 1.7 μJ over the whole spectral tuning range.. The variation of the idler pulse energy versus the wavelength is represented in full downward triangles in Fig. 4d. The idler output pulse energy is about 1 μJ. Note that for idler wavelengths $\lambda_i > 3.5$ μm of high interest for vibrational spectroscopy, there was less than 0.1 μJ. In Fig. 4d, the open circles show the total output pulse energy. Note the corresponding conversion efficiency is weak and about 1.7%.

For KTA crystal, the experimental angle tuning curve is also shown in Fig. 1a (filled triangles). The mismatch of $\approx 2°$ between theoretical and experimental curves could be explained in two ways. On one hand, this mismatch could be due to small errors of the coefficients used in the Sellmeier equations. In fact, several sets of Sellmeier equations were used to calculate the theoretical phase-matching curves. As experimentally observed, we found that only one set of Sellmeier equations was able to nullify the phase mismatch between the three waves in the type-III configuration in the mid-IR range. However, this set does not agree with the experimental data. Therefore, it may be that the Sellmeier equations are to be modified in the mid-IR spectral range. On the other hand, our crystal was very heterogeneous. This implies a poor crystal growth and may explain the deviation with respect to the Sellmeier equations used. In fact in our case, the wide heterogeneity of KTA crystal was a quite limiting factor. For instance, the output pulse energy rapidly changed from point to point in the crystal. Since our data cannot be considered as significant, signal and idler pulse energy measured for the KTA crystal is not reported in this paper. Moreover, the very poor conversion efficiency at the idler wavelength

prevented us from characterizing the idler pulses spectrally and temporally. However, we were able to characterize the signal pulses. Figure 4a shows the temporal (in full upward triangles) and spectral bandwidth (in open circles) of the signal pulses. In this figure, the dashed lines are only a visual guide. There is an almost constant pulse duration of 85 ± 9 fs at FWHM and an increasing spectral bandwidth from 18 to 37 nm at FWHM. The experimental TSBP is 1.0 ± 0.2, which indicates the signal pulses were nearly FTL. A typical spectrum of the signal pulses at 1.02 μm is presented in Fig. 4b. In fact, all the recorded spectra were found to be nearly Gaussian. This is illustrated in Fig. 4b where the open circles show the experimental data and the straight line the related Gaussian fit.

Finally, we studied $KNbO_3$ crystal. The experimental angle tuning curve is reported in Fig. 1b in filled up triangles. The experimental and theoretical angle tuning matching curves do not agree: a mismatch of $\approx 0.5°$ is recorded. We then tested two different $KNbO_3$ crystals produced by the same company but grown separately. Their respective experimental angle tuning curves were found to be quite different. Since according to our crystal supplier the cut angle was accurate up to the first decimal, this seems to indicate that the Sellmeier equations depend on the growth of the crystal. Figure 1b interestingly, shows how this OPA can work on both sides of the angle tuning curve close to the vertical slope. Thus idler wavelengths up to 4.6 μm can be attained. An adjustment of the delay lines was sufficient to make our OPA pass from one side to the other side of this turning back point. Figure 5a,b shows the evolution of the signal (in Fig. 5a) and idler (in Fig. 5b) pulse duration (in filled triangles) as well as their spectral bandwidths (in open circles) along the phase-matching curves. In these figures, dashed lines are only a visual guide. For both signal and idler, the pulse duration was constant over the whole spectral tuning range. It was found to be ≈ 100 fs at FWHM. The spectral bandwidth at FWHM increased from 30 to 95 nm for signal and from 70 to 180 nm for idler pulses. All the recorded spectra were found to be nearly Gaussian. A typical idler spectrum centered at 4.6 μm

Fig. 5a–d. OAP experimental results obtained with $KNbO_3$. **a ,b** Pulse durations at FWHM in *full upward triangles* and their spectral bandwidth at FWHM in *open cicles* are reported for signal and idler pulses, respectively. *Dashed lines* are only visual guides.**c** Total, signal, and idler output pulse energies are respectively plotted in *open circles*, *full upward* and *downward triangles*.**d** An experimental idler spectrum (in *open circles*) centered at 4.6 μm with its Gaussian fit (*straight lines*) is presented

is shown in Fig. 5d (open circles) along with a Gaussian fit (straight line). Our experimental data were used to extrapolate at 100 fs the temporal width of such an idler pulse, it would only contain 6.5 optical cycles. The TSBP is equal to 1.8 ± 0.3 for signal, and to 1.2 ± 0.4 for idler pulses. Therefore neither signal nor idler pulses are FTL. According to their spectra, such pulses could be recompressed up to 56 fs for signal and up to 83 fs for idler. The deviation of the TSBP from unity is certainly related to the large spectral acceptance of $KNbO_3$ crystal and the chirp of the seeding white-light continuum. Note that idler pulses were better FTL than signal pulses. This can be explained by the group velocities dispersion (GVD) in $KNbO_3$ crystal which leads to an opposite GVD sign between signal and idler pulses. For idler pulses, the GVD compensates the continuum chirp and gives almost FTL pulses whereas, for signal pulses, the effects of GVD increase the continuum chirp and signal pulses become lesser FTL. Finally, we measured signal, idler, and total output pulse energies. They are respectively plotted in open circles and full upward and downward triangles in Fig. 5c. Over the whole spectral tuning range, the signal and idler output pulses energy was $\approx 10.5\,\mu J$ and $\approx 5\,\mu J$, respectively. More than $3\,\mu J$ was generated in the 4–4.6 μm mid-IR region. Over the whole spectral range, the conversion efficiency was $\approx 11.5\%$.

During all these experiments, for both KTP and $KNbO_3$ crystals, the shot-to-shot and day-to-day stability of the output pulse energy was very high and about $\pm 2\%$. Such a high reliability is mainly related to the stability of the Ti:sapphire regenerative amplifier.

4 Conclusion

We have designed a simple mid-IR fs OPA delivering very stable, largely tunable and energetic output pulses which requires less than $200\,\mu J$ pump pulse energy. The same experimental conditions have been used to compare the performances of potassium-based KTP, KTA, and $KNbO_3$ crystals for the generation of mid-IR wavelengths in the fs regime. The KTA crystal allows the generation of 100-fs FTL pulses in the near-IR spectral range. For KTP, the ≈ 100 fs output pulse energy was low ($\approx 1.7\,\mu J$ for signal and $\approx 1\,\mu J$ for idler with less than $0.1\,\mu J$ in the mid-IR range) and was nearly FTL. Finally, the pulses generated by the $KNbO_3$ crystal were more energetic ($\approx 10.5\,\mu J$ for signal and $\approx 5\,\mu J$ for idler with more than $3\,\mu J$ in the mid-IR) but were not perfectly FTL due to the large spectral acceptance. Therefore we conclude that due to its large effective susceptibility and great tunability, the $KNbO_3$ crystal is one of the best potassium-based crystals for a powerful 100-fs OPA designed to study time-resolved vibrational spectroscopy in the MIR spectral range.

References

1. V. Petrov, F. Noack: Opt. Lett. **21**, 1576 (1996)
2. G.M. Gale, G. Gallot, F. Hache, R. Sander: Opt. Lett. **22**, 1253 (1997)
3. J.D. Kafka, M.L. Watts: *Ultrafast Phenomena X*, Springer Series in Chem. Phys. **62**, 38 (1996)
4. V. Petrov, F. Noack, R. Stolzenberger: Appl. Opt. **36**, 1164 (1997)
5. V. Petrov, F. Noack: J. Opt. Soc. Am. B **12**, 2214 (1995)
6. G.R. Holtom, R.A. Crowell, X.S. Xie: J. Opt. Soc. Am. B **12**, 1723 (1995)
7. V.G. Dmitriev, G.G. Gurzadyan, D.N. Nikogosyan: *Handbook of Nonlinear Optical Crystals*, second revised and updated edn. / Springer Series in Optical Science, Vol. 64, (1997)
8. H. Vanherzeele, J.D. Bierlein, F.C. Zumsteg: Appl. Opt. **27**, 3314 (1988)
9. K. Kato: IEEE J. **30**, 881 (1994)
10. B. Zysset, I. Biaggio, P. Günter: J. Opt. Soc. Am. B **9**, 380 (1992)
11. H. Vanherzeele: Appl. Opt. **29**, 2246 (1990)